Wu et al. *EPJ Quantum Technology* (2024) 11:88
https://doi.org/10.1140/epjqt/s40507-024-00301-6

EPJ Quantum Technology
a SpringerOpen Journal

EPJ.org

RESEARCH Open Access

Nonreciprocal mechanical squeezing in cavity magnomechanics

Hao-Tian Wu[1], Ping-Chi Ge[1], Xue Han[1*], Hong-Fu Wang[1*] and Shou Zhang[1*]

*Correspondence:
xuehan@ybu.edu.cn;
hfwang@ybu.edu.cn;
szhang@ybu.edu.cn
[1]Department of Physics, College of Science, Yanbian University, 133002 YanJi, JiLin, China

Abstract

We propose a scheme to achieve nonreciprocal mechanical squeezing in a hybrid Kerr-modified cavity magnomechanical system, where the magnon mode is driven by two-tone microwave fields. The nonreciprocity originates from the magnon Kerr effect. Strong mechanical squeezing beyond the 3 dB limit can be nonreciprocally generated by adjusting the magnon frequency detuning, effective magnomechanical coupling strength, as well as the damping of the oscillator and the dissipation of the cavity. Importantly, the proposed scheme is robust against environmental thermal noise and system dissipation, ensuring its feasibility under current experimental conditions. This work may pave the way for the development of nonreciprocal quantum devices, such as isolators and circulators. Furthermore, the ability to achieve such robust mechanical squeezing has significant implications for advancing quantum precision measurements in metrology and sensing, offering new opportunities for exploring quantum-enhanced technologies.

Keywords: Mechanical squeezing; Nonreciprocal physics; Cavity magnomechanics

1 Introduction

Hybrid systems based on magnons have garnered significant interest for their potential in advancing novel quantum technologies [1–3]. Among these, cavity magnomechanics (CMM)—which involves coupling a ferrimagnetic crystal, such as yttrium iron garnet (YIG, $Y_3Fe_5O_{12}$) with a microwave cavity, has attracted considerable attention in recent years [4–7]. In these systems, magnons couple with photons via magnetic-dipole interactions [8], and with phonons through magnetostrictive interactions [9]. This multimodal coupling enables the integration of magnon, photon, and phonon modes, offering a versatile platform for exploring a wide range of quantum phenomena. A variety of physical effects have been demonstrated both theoretically and experimentally in CMM systems, including magnomechanically induced transparency [10–12], quantum entanglement [13–15] and one-way quantum steering [16–18], mechanical bistability [19], magnon blockade [20–22], magnon dark mode [23, 24], precision measurement [25–27] and sensing [28–30]. Notable studies have also explored the Kerr effect in magnons [19, 31, 32], along with phonon and magnon squeezing [33–37].

Springer

Squeezed states are fundamental quantum resources, critical for continuous-variable information processing. They play a pivotal role in enhancing measurement sensitivity, with promising applications in quantum information science and quantum metrology [38, 39]. Various methods for generating squeezed states have been developed across different platforms, and the CMM system has emerged as a particularly promising candidate for such investigations [40, 41]. Specifically, magnon and phonon squeezing in CMM systems can be achieved using techniques such as Josephson parametric amplification (JPA) [42, 43], Duffing nonlinearity [44, 45], two-tone laser driving [46, 47]. Among these, two-tone driving has been proven especially effective for eliciting rich quantum properties and dynamics.

Nonreciprocal physics, which examines phenomena where a system exhibits different behaviors in opposite directions, has garnered significant attention in recent years [48]. Quantum nonreciprocal effects cause wide concern, with the potential to advance both fundamental physics and quantum technologies, including quantum information processing and quantum computing [49–52]. One of the most exciting topics currently under investigation is nonreciprocal squeezing, achieved by breaking time-reversal symmetry (e.g., by modulating the magnetic field direction), which causes the system to exhibit different quantum squeezing effects in different directions [53]. In cavity optomechanical (COM) system, nonreciprocal mechanical squeezing can be achieved by utilising spinning cavity. This effect arises from the Sagnac-Fizeau effect, where the spinning cavity induces opposite frequency shifts, allowing mechanical squeezing in one drive direction but not in the reverse [54, 55]. The magnon Kerr effect provides another avenue for exploring nonreciprocal quantum phenomena in CMM systems, such as nonreciprocal photon-phonon entanglement [1, 56]. By tuning the direction of the magnetic field applied along the crystal axes [100] or [110], a positive or negative frequency shift is generated, enabling the realization of nonreciprocal quantum effects. The alteration of the magnetic field's direction can be achieved by modifying the orientation of the current in the magnetic field coils, indirectly influencing the distribution and interactions of the magnetic field [57].

Inspired by the above work, here we propose a scheme to achieve nonreciprocal mechanical squeezing in a hybrid Kerr-modified CMM system. The magnon Kerr effect enables mechanical squeezing to occur when the magnetic field is applied in one direction but not in the opposite direction. We investigate the influence of the magnomechanical coupling strength and magnon frequency detuning on the nonreciprocal squeezing behavior, demonstrating that ideal nonreciprocal squeezing is achievable within experimentally feasible parameters. Furthermore, we examine the effects of intrinsic losses and thermal noise, showing that the proposed scheme remains robust against both types of dissipation.

This paper is organized as follows. In Sect. 2, we introduce the hybrid Kerr-modified CMM system, driven by two-tone laser, and present the system Hamiltonian in detail. In Sect. 3, we analyze the dynamical evolution of quantum fluctuation in the system. In Sect. 4, we explore nonreciprocal mechanical squeezing and provide a detailed discussion of its underlying physical mechanism. Finally, we give a brief summary of our work in Sect. 5.

2 Model and Hamiltonian

We consider a hybrid Kerr-modified CMM system as shown in Fig. 1(a), which consists of a microwave cavity, and a YIG sphere supporting a Kittle mode is positioned in a static

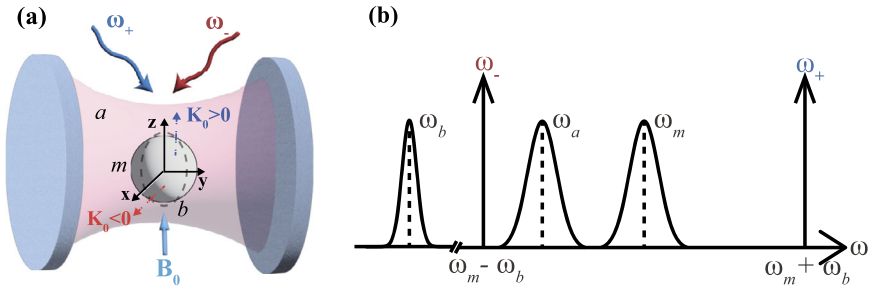

Figure 1 (a) Device sketch of Kerr-modified CMM system. The YIG sphere is placed in a microwave cavity and the two-tone laser directly drives the magnon mode of the YIG sphere to obtain squeezing. In addition, the Kittel mode is driven by a magnetic field, and by changing the driving direction of the magnetic field, the positive and negative of K_0 can be changed, leading to the generation of nonreciprocal phenomena. (b) Frequency spectrum of the hybrid Kerr-modified CMM system

magnetic field B_0. The Kerr magnon in the Kittel mode of the YIG sphere couples to microwave cavity photons via magnetic dipole interaction and to the vibrational phonons of the YIG sphere via magnetostrictive interaction, respectively. The magnon mode is driven by a two-tone laser with different amplitudes $E_\pm$ and frequencies $\omega_\pm$. The total Hamiltonian of the system (in the unit of $\hbar = 1$) is given by

$$H = H_0 + H_{\text{kerr}} + H_{\text{int}} + H_{\text{d}}, \tag{1}$$

where

$$H_0 = \omega_a a^\dagger a + \omega_b b^\dagger b,$$
$$H_{\text{Kerr}} = \omega_m m^\dagger m + K_0 (m^\dagger m)^2,$$
$$H_{\text{int}} = g_a (a^\dagger m + a m^\dagger) + g_b m^\dagger m (b^\dagger + b),$$
$$H_{\text{d}} = (E_+ e^{-i\omega_+ t} + E_- e^{-i\omega_- t}) m^\dagger + \text{H.c.}$$

Here a ($a^\dagger$), b ($b^\dagger$), and m ($m^\dagger$) are respectively the annihilation (creation) operators of photon, phonon and magnon, which satisfying the commutator relation $[\sigma, \sigma^\dagger] = 1$ ($\sigma = a, b$ and m). ω_a, ω_b and ω_m are the frequency of cavity mode, mechanical mode and Kittel mode, respectively. The coupling strength between the cavity mode and the Kittel mode, denoted by g_a, and the magnon-phonon coupling strength, denoted by g_b. In the absence of an external driving field, the magnomechanical coupling strength g_b is typically weak. However, it can be enhanced by applying a driving field to the Kittel mode. Here, two lasers with the frequency $\omega_\pm = \omega_m \pm \omega_b$ and the amplitudes $E_\pm$ are employed to drive the Kittel mode. The K_0 term describes the magnon Kerr nonlinearity in the Kittel mode of the YIG sphere, which is caused by magnetocrystalline anisotropy. Experimentally, the Kerr coefficient K_0, which is inversely proportional to the volume of the YIG sphere, can be tuned within the range of 0.05 to 100 nH by varying the sphere's diameter from 1 mm to 100 μm and adjusted positively or negatively by changing the direction of the applied magnetic field [19, 32]. In other words, when the magnetic field is aligned along the crystal axis in the direction [100], K_0 is positive. Conversely, when the magnetic field is aligned along the crystal axis in the direction [110], K_0 is negative.

By incorporating considerations of mechanical damping, cavity decay, and environmental noise, the dynamics of the CMM system can be described by the following nonlinear quantum Langevin equations (QLEs)

$$\begin{aligned}
\dot{a} &= -(i\omega_a + \frac{\kappa_a}{2})a - ig_a m + \sqrt{\kappa_a}a_{in},\\
\dot{b} &= -(i\omega_b + \frac{\gamma_b}{2})b - ig_b m^\dagger m + \sqrt{\gamma_b}b_{in},\\
\dot{m} &= -(i\omega_m + \frac{\kappa_m}{2})m - ig_b m(b^\dagger + b) - 2iK_0 m^\dagger mm\\
&\quad -ig_a a - i(E_+ e^{-i\omega_+ t} + E_- e^{-i\omega_- t}) + \sqrt{\kappa_m}m_{in},
\end{aligned} \tag{2}$$

where κ_a, γ_b, and κ_m, respectively, represent the decay rates of cavity mode, phonon mode, and Kittel mode. σ_{in} is the input noise operator corresponding to the three modes with the nonzero correlation functions [58]

$$\begin{aligned}
\langle \sigma_{\rm in}(t)\sigma_{\rm in}^\dagger(t')\rangle &= (n_\sigma + 1)\delta(t-t'),\\
\langle \sigma_{\rm in}^\dagger(t')\sigma_{\rm in}(t)\rangle &= n_\sigma \delta(t-t'),
\end{aligned} \tag{3}$$

where $n_\sigma = [\exp(\hbar\omega_\sigma/k_B T) - 1]^{-1}$ is the mean thermal excitation number of three modes when the environmental temperature is T, and k_B is the Boltzmann constant.

The standard linearization relation can be employed to rewrite the operators in the form of the steady-state mean plus quantum fluctuation (i.e., $\dot{\sigma} = \dot{\sigma}_s + \dot{\delta}\sigma$). Substituting this into Eq. (2) yields:

$$\begin{aligned}
\delta\dot{a} &= -(i\omega_a + \frac{\kappa_a}{2})\delta a - ig_a \delta m + \sqrt{\kappa_a}a_{in},\\
\delta\dot{b} &= -(i\omega_b + \frac{\gamma_b}{2})\delta b - ig_b(m_s^*\delta m + m_s\delta m^\dagger) + \sqrt{\gamma_b}b_{in},\\
\delta\dot{m} &= -i[\omega_m + g_b(b_s^* + b_s) + 2\Delta_k]\delta m - \frac{\kappa_m}{2}\delta m - i\Delta_k\delta m^\dagger\\
&\quad -ig_a\delta a - ig_b m_s(\delta b^\dagger + \delta b) + \sqrt{\kappa_m}m_{in},
\end{aligned} \tag{4}$$

and

$$\begin{aligned}
\dot{a}_s &= -(i\omega_a + \frac{\kappa_a}{2})a_s - ig_a m_s,\\
\dot{b}_s &= -(i\omega_b + \frac{\gamma_b}{2})b_s - ig_b|m_s|^2,\\
\dot{m}_s &= -[i(\omega_m + \Delta_k) + \frac{\kappa_m}{2}]m_s - ig_a a_s - ig_b m_s(b_s^* + b_s)\\
&\quad -i(E_+ e^{-i\omega_+ t} + E_- e^{-i\omega_- t}),
\end{aligned} \tag{5}$$

where $\Delta_k = 2K_0|m_s|^2$ is the frequency shift caused by the Kerr effect. Since the amplitude of the Kittel mode is dominant at the two-tone drive frequencies $m_\pm$, we assume that $m_s(t) \approx m_+ e^{-i\omega_+ t} + m_- e^{-i\omega_- t}$ and $a_s(t) \approx a_+ e^{-i\omega_+ t} + a_- e^{-i\omega_- t}$. Moreover, since the magnomechanical coupling g_b is very small in the current CMM experiment, the $g_b(b_s^* + b_s)$ term in

the above equation can be ignored. In this way, we obtain the mean amplitudes $m_{\pm}$, which are associated with the Kittel mode:

$$m_{\pm} = \frac{E_{\pm}}{\pm\omega_b + \Delta_k + i\frac{\kappa_m}{2} - \frac{g_a^2}{\omega_{\pm}-\omega_a+i\frac{\kappa_a}{2}}}. \tag{6}$$

To simplify the calculation, the linearization Hamiltonian can be obtained from Eq. (4). Furthermore, using the rotating frame $U = e^{-i[\omega_a(a^\dagger a+m^\dagger m)+\omega_b b^\dagger b]t}$, we can obtain the linearization Hamiltonian in the interaction picture

$$\begin{aligned} H_{eff} &= (\Delta_m + 2\Delta_k)\delta m^\dagger \delta m + g_a(\delta a\delta m^\dagger + \delta a^\dagger \delta m) + [\delta m^\dagger(G_+\delta b^\dagger + G_-\delta b) \\ &\quad +\delta m^\dagger(e^{-2i\omega_b t}G_+\delta b + e^{2i\omega_b t}G_-\delta b^\dagger) + \text{H.c.}], \end{aligned} \tag{7}$$

where $\Delta_m = \omega_m - \omega_a$ is the detuning of the Kittel mode frequency with respect to the cavity mode frequency. $G_{\pm} = g_b m_{\pm}$ represent the effective magnomechanical coupling strengths associated with the drive fields. Without loss of generality, we assume $G_{\pm} > 0$ to be real.

3 Dynamics of quantum fluctuations

Now, to further study the dynamics of quantum fluctuation, since $\kappa_{m(a)}, g_a, G_{\pm} \ll \omega_b$, using the rotating wave approximation (RWA), the above equation can be written in the form of linearization QLEs

$$\begin{aligned} \delta\dot{a} &= -\frac{\kappa_a}{2}\delta a - ig_a\delta m + \sqrt{\kappa_a}a_{\text{in}}, \\ \delta\dot{b} &= -\frac{\gamma_b}{2}\delta b - i(G_-\delta m + G_+\delta m^\dagger) + \sqrt{\gamma_b}b_{\text{in}}, \\ \delta\dot{m} &= -[i(\Delta_m + 2\Delta_k) + \frac{\kappa_m}{2}]\delta m - i\Delta_k\delta m^\dagger \\ &\quad -ig_a\delta a - i(G_-\delta_b + G_+\delta_{b^\dagger}) + \sqrt{\kappa_m}m_{in}, \end{aligned} \tag{8}$$

in order to investigate mechanical squeezing, we define a pair of quadrature operators of quantum fluctuations and their corresponding noise operators as $\delta X_\sigma = (\delta\sigma + \delta\sigma^\dagger)/\sqrt{2}$, $\delta Y_\sigma = (\delta\sigma - \delta\sigma^\dagger)/i\sqrt{2}$, and $X_{\sigma_{\text{in}}} = (\sigma_{\text{in}} + \sigma_{\text{in}}{}^\dagger)/\sqrt{2}$, $Y_{\sigma_{\text{in}}} = (\sigma_{\text{in}} - \sigma_{\text{in}}{}^\dagger)/i\sqrt{2}$, all quadrature operators can be represented as column vectors $\mathbf{u}(t) = [\delta X_a(t), \delta Y_a(t), \delta X_b(t), \delta Y_b(t), \delta X_m(t), \delta Y_m(t)]^T$, and $\mathbf{N}(t) = [\sqrt{\kappa_a}X_{a_{in}}, \sqrt{\kappa_a}Y_{a_{in}}, \sqrt{\gamma_b}X_{b_{in}}, \sqrt{\gamma_b}Y_{b_{in}}, \sqrt{\kappa_m}X_{m_{in}}, \sqrt{\kappa_m}Y_{m_{in}}]^T$. Then, the linearized QLEs in Eq. (8) governing the dynamics of the quantum fluctuations can be written in a compact form [59]

$$\dot{\mathbf{u}}(t) = \mathbf{A}(t)\mathbf{u} + \mathbf{N}(t), \tag{9}$$

where $\mathbf{A}(t)$ is the drift matrix is given by

$$\mathbf{A}(t) = \begin{pmatrix} -\frac{\kappa_a}{2} & 0 & 0 & 0 & 0 & g \\ 0 & -\frac{\kappa_a}{2} & 0 & 0 & -g & 0 \\ 0 & 0 & -\frac{\gamma_b}{2} & 0 & 0 & G_- - G_+ \\ 0 & 0 & 0 & -\frac{\gamma_b}{2} & -(G_- + G_+) & 0 \\ 0 & g & 0 & G_- - G_+ & -\frac{\kappa_m}{2} & \Delta_m + \Delta_k \\ -g & 0 & -(G_- + G_+) & 0 & -\Delta_m - 3\Delta_k & -\frac{\kappa_m}{2} \end{pmatrix}. \tag{10}$$

The linearized evolution of quantum fluctuations and the zero-mean Gaussian property of quantum noise result in the asymptotic quantum state of the system evolving into a Gaussian state that is independent of the initial state [60]. This asymptotic quantum state can be characterized by a 6×6 covariance matrix (CM) V, with the elements of which are defined as follows:

$$V_{kl} = \langle u_k(t)u_l(t) + u_l(t)u_k(t)\rangle /2. \tag{11}$$

The CM V can be obtained by solving the Lyapunov equation directly,

$$\dot{\mathbf{V}} = A(t)V(t) + V(t)A(t)^T + D, \tag{12}$$

here, the symbol D represents the diffusion matrix $D = \mathrm{diag}[\kappa_a(2n_a + 1), \kappa_a(2n_a + 1), \gamma_b(2n_b + 1), \gamma_b(2n_b + 1), \kappa_m(2n_m + 1), \kappa_m(2n_m + 1))]$, whose elements are related to the noise correlation function and are typically defined by $\delta(t - t')D_{k,l} = \left\langle n_k(t)n_l(t') + n_l(t')n_k(t)\right\rangle /2$. Furthermore, in order to guarantee the stability of the system, in accordance with the Routh-Hurwitz criterion, it is essential to ensure that all eigenvalues of the matrix $\mathbf{A}(t)$ have a negative real part [61].

4 Nonreciprocal mechanical squeezing with Kerr effect

Next we are interested in investigating the properties and the phenomena of mechanical quadrature squeezing, according to the Heisenberg uncertainty principle the degree of squeezing can be defined in the dB unit

$$\mathcal{S} = -10\log_{10}\frac{\left\langle \delta O^2\right\rangle}{\left\langle \delta O^2\right\rangle_{vac}}, \tag{13}$$

where $\left\langle \delta O^2\right\rangle_{vac} = \frac{1}{2}$ $(O = X, Y)$ is the vacuum fluctuation, and $\left\langle \delta O^2\right\rangle$ denotes the diagonal element of the covariance matrix. When $\mathcal{S} > 0$, it means that the corresponding mode is squeezed, and when $\mathcal{S} > 3$, strong squeezing is generated.

In order to study nonreciprocal squeezing, the following parameters are employed in experimentally accessible manners [3, 11, 62]: $\omega_a = 2\pi \times 10$ GHz, $\omega_b = 2\pi \times 30$ MHz, $\kappa_a = \kappa_m = 2\pi$ MHz, $\gamma_b = 2\pi \times 100$ Hz, $g = G_- = 2\pi \times 3$ MHz, $T = 10$ mK. To achieve nonreciprocal mechanical squeezing in the hybrid Kerr-modified CMM system, i.e., the mechanical squeezing can be generated by driving the Kittel mode along the crystal axis [110] but not the [100], we numerically calculate the variance of the phase quadrature of the mechanical mode $\left\langle \delta {X_b}^2\right\rangle$ and the evolution of the steady-state variance is plotted in Fig. 2. The red line and green line represent the variance for the $K_0 < 0$ and $K_0 > 0$ cases, respectively. It is evident that the variance of the quadrature of the mechanical mode is squeezed when the direction of the driving Kittel mode is [110]. However, when the direction of driving Kittel mode is [100], no mechanical squeezing occurs. That is, nonreciprocal mechanical squeezing can be achieved in this hybrid Kerr-modified CMM system. Furthermore, it is possible to achieve a mechanical squeezing of greater than 3 dB in different directions by selecting the appropriate parameters. This phenomenon is related to the anti-Stokes sideband cooling corresponding to the red detuned driving field, the more detailed examination of the physical mechanisms will be provided in the subsequent discussion.

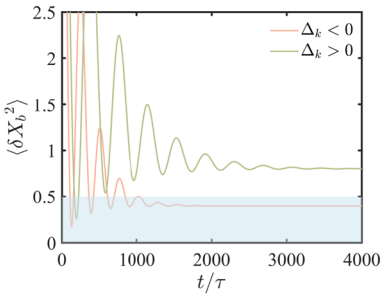

Figure 2 The time evolution of the variance of the phase quadrature of the mechanical mode $\langle \delta X_b{}^2 \rangle$ with $\Delta_k < 0$ and $\Delta_k > 0$. The parameters are $G_+ = 0.96G_-$, $\Delta_k = 0.5\omega_b$ and $\Delta_m = 5\omega_b$. See text for other parameters. The blue region of the graph represents the area below the quantum noise limit, indicating the presence of quantum squeezing in this region. This figure highlights the difference in the time evolution of the mechanical mode's phase quadrature variance under different Δ_k conditions

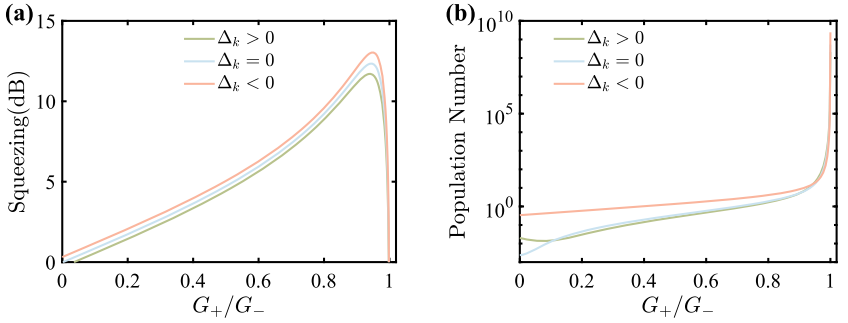

Figure 3 (a) The degree of squeezing $\mathcal{S}$ and (b) The population number of the mechanical mode versus the ratio of effective magnomechanical coupling strengths G_+/G_- with $\Delta_k > 0$, $\Delta_k = 0$ and $\Delta_k < 0$. The parameters are $\Delta_k = 0.3\omega_b$ and $\Delta_m = \omega_b$. The other parameters are the same as those in Fig. 2. This figure shows how the squeezing and population dynamics of the mechanical mode depend on the relative magnomechanical coupling strength ratio with different Δ_k

In order to illustrate the impact of the effective magnomechanical coupling strength on the degree of squeezing, we plot the variation of mechanical squeezing with the ratio of coupling strengths in Fig. 3(a). It can be seen that regardless of whether the value of Δ_k is positive or negative, the mechanical squeezing increases and then decreases with the ratio of G_+/G_-. Furthermore, it can be demonstrated that there exists an optimal ratio that maximises the degree of squeezing. This phenomenon can be attributed to the competitive relationship between the squeezing and cooling. The population number of mechanical mode is plotted as a function of the ratio of G_+/G_- in Fig. 3(b). It can be observed that as the G_+/G_- ratio increases, the cooling effect of the oscillator diminishes until it cannot be effectively cooled to the ground state. This is one of the factors that contributes to the variability in the degree of squeezing.

The mechanism by which two-tone driven fields influence the physical process in Fig. 3 can be described in detail as follows: the effective Hamiltonian resulting from the RWA is derived from Eq. (8), by introducing the Bogoliubov mode corresponding to the mechanical mode $\delta\beta = \cosh(r)\delta b + \sinh(r)\delta b^\dagger$, where r is squeezing parameter defined by $\tanh r = G_+/G_-$. The direct magnetostrictive force between the Kittel mode and the phonon mode of the YIG is given by the following equation

$$H_{int} = \mathcal{G}(\delta m^\dagger \delta\beta + \delta m \delta\beta^\dagger), \tag{14}$$

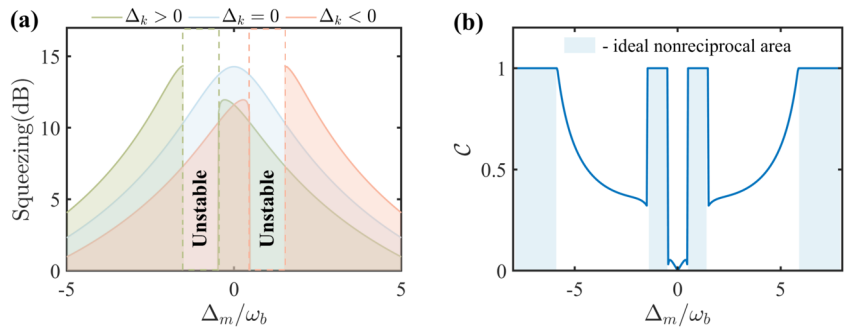

Figure 4 (a) The degree of squeezing $\mathcal{S}$ of the mechanical mode versus the magnon frequency detuning Δ_m/ω_b with $\Delta_k > 0$, $\Delta_k = 0$ and $\Delta_k < 0$. The regions of the dotted line are unstable areas. (b) The chiral factors for mechanical squeezing as a function of detuning Δ_m/ω_b, and the blue areas represent the ideal nonreciprocal areas. The parameters are $\Delta_k = 0.5\omega_b$ and $\Delta_m = 5\omega_b$. The other parameters are the same as those in Fig. 2. This figure demonstrates how the mechanical mode squeezing and the chiral factors evolve with Δ_k

where $\mathcal{G} = \sqrt{G_-^2 - G_+^2}$ is the coupling strength between Bogoliubov mode and Kittel mode. The above equation represents the well-known beam-splitter-like interaction in sideband cooling. It can be demonstrated that the Bogoliubov mode β can be cooled by the magnon dissipation κ_m according to the reservoir engineering mechanism. However, the competition arises from the interplay between the increase of the squeezing parameter r and the reduction of the beam-splitter-like interaction strength $\mathcal{G}$ as G_+ increases. Consequently, a trade-off between these two competing factors results in the optimal degree of squeezing.

In addition to the influence of effective magnomechanical coupling strengths G_+ and G_- on mechanical squeezing, the change of detuning also affects nonreciprocal squeezing. This is demonstrated in Fig. 4(a), which plots the degree of squeezing as a function of detuning in different magnetic field drive directions. The blue line represents the degree of mechanical squeezing of the mode in the absence of the Kerr effect, that is, when $K_0 = 0$. The green and red lines represent the mechanical squeezing that occurs when the magnetic field drives the Kittel mode along the crystal axes [110] and [100] directions, (i.e., $\Delta_k > 0$ and $\Delta_k < 0$) respectively, which demonstrates the nonreciprocity of the mechanical squeezing. It should be noted that in order to determine the stability of the system, there are regions of unstability in the system when both $K_0 > 0$ and $K_0 < 0$. This can be demonstrated by applying the Routh-Hurwitz criterion. Moreover, in order to provide a quantitative description of the nonreciprocity of mechanical squeezing, we introduce the chiral factor $\mathcal{C}$ as follows

$$\mathcal{C} = \left| \frac{\mathcal{S}(\Delta_k > 0) - \mathcal{S}(\Delta_k < 0)}{\mathcal{S}(\Delta_k > 0) + \mathcal{S}(\Delta_k < 0)} \right|, \tag{15}$$

where chiral factor $\mathcal{C}$ should be within the range of 0 to 1, corresponding to weak to strong nonreciprocity of mechanical squeezing. When $\mathcal{C} = 1$, this represents the ideal nonreciprocal case. In Fig. 4(b), the chiral factor $\mathcal{C}$ is plotted against the frequency detuning Δ_m, here the blue region represents the ideal nonreciprocal area, which occurs when the amount of detuning is sufficiently large. Additionally, the ideal nonreciprocal area also occurs when the detuning is approximately equal to zero, which corresponds to the unstability area in Fig. 4(a). It is evident that the chiral factor is significantly correlated with

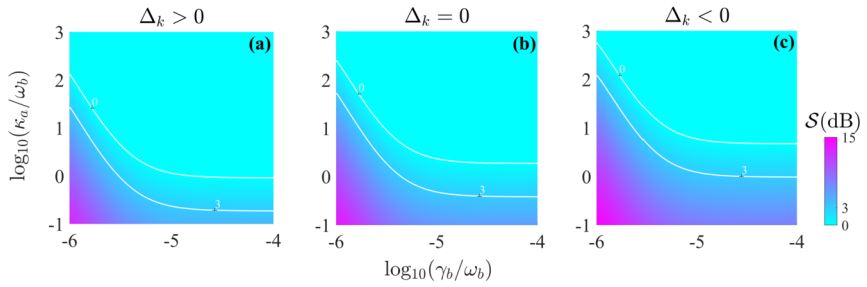

Figure 5 The degree of squeezing versus the dissipation of cavity mode κ_a and damping of mechanical mode γ_b with $\Delta_k > 0$, $\Delta_k = 0$ and $\Delta_k < 0$. We take $\Delta_k = 0.1\omega_b$ and $\Delta_m = \omega_b$. The other parameters are the same as those in Fig. 2. The contour lines with values of 0 and 3 correspond to the range where squeezing exists ($\mathcal{S} > 0$) and the region where strong squeezing occurs ($\mathcal{S} > 3$), respectively. The figure demonstrates how the degree of squeezing is influenced by the cavity dissipation and mechanical damping under varying Δ_k conditions

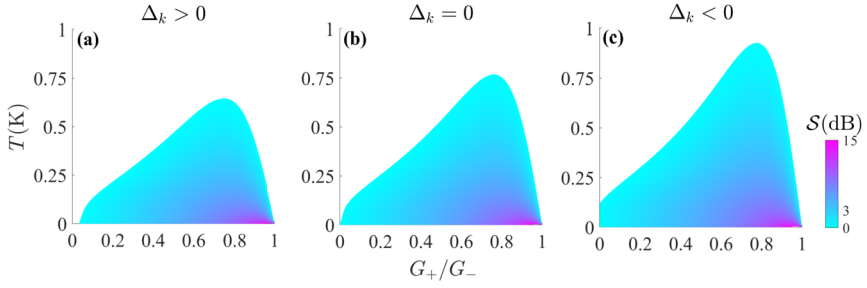

Figure 6 The degree of squeezing versus temperature T and the ratio of effective magnomechanical coupling strengths G_+/G_- with $\Delta_k > 0$, $\Delta_k = 0$ and $\Delta_k < 0$. The other parameters are the same as those in Fig. 5. The blank areas represent the regions where no squeezing occurs

detuning, and the chiral factor $\mathcal{C}$ can be altered from 0 to 1 by varying the detuning. This demonstrates that the ideal nonreciprocal squeezing effect can be achieved in our scheme by modifying the frequency detuning of the Kittel mode.

From a practical standpoint, the dissipation is an unavoidable consequence in the CMM system. Nevertheless, given that the magnon mode decay rate remains relatively constant for a YIG sphere constrained by intrinsic loss, we will now focus on the influence of the dissipation of the cavity mode and the damping of the phonon mode on mechanical squeezing. Experiments have shown that varying the environmental pressure (e.g., operating in vacuum conditions) can minimize mechanical damping [63]. Additionally, using superconducting or high-reflectivity coatings can minimize dissipation of cavity, thereby improving the cavity's quality factor [64]. In Fig. 5, we plot the steady-state degree of squeezing $\mathcal{S}$ versus the decay rates κ_a and γ_b. It can be seen that mechanical squeezing can be achieved over a wide range of κ_a and γ_b, regardless of the value of K_0. Furthermore, when Δ_k is negative, the system's dissipation requirements are most relaxed, and strong mechanical squeezing can be observed even within a wide range of parameter values. In addition to the losses of the system, another factor that has a non-negligible impact on the system in practice is the temperature. We plot the variation of mechanical squeezing with temperature and coupling ratio G_+/G_- in Fig. 6. Similar to the effect of system's dissipation on squeezing, mechanical squeezing is most robust to temperature when $\Delta_k < 0$, even

near 0.9 K. The preceding discussion demonstrates that by selecting parameters that are experimentally feasible, our scheme can achieve nonreciprocal mechanical squeezing in practice. In comparison to the previous scheme, which employed the Sagnac–Fizeau effect to generate nonreciprocal squeezing [54, 55], the present approach achieves a higher degree of mechanical squeezing and demonstrates greater robustness against thermal noise and system dissipation.

5 Conclusions

In conclusion, we have investigated the nonreciprocal mechanical squeezing in a hybrid Kerr-modified CMM system. The Kerr effect enables nonreciprocal mechanical squeezing by applying a magnetic field to the Kittel mode of the YIG sphere from different directions. Our scheme has demonstrated that both the effective magnomechanical coupling strengths and frequency detuning have a large impact on mechanical squeezing. Furthermore, the influence of the system dissipation and the external environment on mechanical squeezing can be significantly reduced with the appropriate system parameters. Notably, all the chosen parameters are experimentally feasible and enable the realization of strong mechanical squeezing, exceeding the 3 dB standard quantum limit. Consequently, this work offers a valuable tool for investigating quantum nonreciprocity and provides a novel approach for advancing quantum precision measurements.

Abbreviations

CMM, cavity magnomechanics; YIG, yttrium iron garnet; JPA, Josephson parametric amplification; COM, cavity optomechanical; QLEs, quantum Langevin equations; RWA, rotating wave approximation; CM, covariance matrix.

Author contributions

H.T.W., X.H., H.F.W. and S.Z. initiated the project and wrote the manuscript. P.C.G. provided expertise on the theoretical analysis. X.H., H.F.W. and S.Z. supervised the project. All authors discussed the results and contributed to the final manuscrip

Funding

This work was supported by the National Natural Science Foundation of China under Grants Nos. 62101479, 62475226, 62071412, 12074330, and 12375020; the Natural Science Foundation of Jilin Province under Grant No. 20240101013JC; and the Young Talents Support Project of Association of Science and Technology of Jilin Province under Grant No. QT202425.

Data Availability

No datasets were generated or analysed during the current study.

Declarations

Ethics approval and consent to participate

Not applicable.

Competing interests

The authors declare no competing interests.

Received: 16 November 2024 Accepted: 17 December 2024 Published online: 20 December 2024

References

1. Chen J, Fan XG, Xiong W, Wang D, Ye L. Nonreciprocal photon-phonon entanglement in Kerr-modified spinning cavity magnomechanics. Phys Rev A. 2024;109:043512.
2. Kong D, Xu J, Wang F. Nonreciprocal entanglement of ferrimagnetic magnons and nitrogen-vacancy-center ensembles by Kerr nonlinearity. Phys Rev Appl. 2024;21:034061.
3. Shen RC, Li J, Fan ZY, Wang PY, You JQ. Mechanical bistability in Kerr-modified cavity magnomechanics. Phys Rev Lett. 2020;129:123601.
4. Li J, Zhu SY, Agarwal GS. Magnon-photon-phonon entanglement in cavity magnomechanics. Phys Rev Lett. 2018;121:203601.
5. Van Kranendonk J, Van Vleck JH. Spin waves. Rev Mod Phys. 1958;30:1.

6. Yuan HY, Cao YS, Kamra A, Duine RA, Yan P. Quantum magnonics: when magnon spintronics meets quantum information science. Phys Rep. 2022;965:1–74.
7. Jiao YF, et al. Nonreciprocal optomechanical entanglement against backscattering losses. Phys Rev Lett. 2020;125:143605.
8. Chen YT, Du L, Zhang Y, Wu JH. Perfect transfer of enhanced entanglement and asymmetric steering in a cavity-magnomechanical system. Phys Rev A. 2021;103:053712.
9. Li J, Zhu SY. Entangling two magnon modes via magnetostrictive interaction. New J Phys. 2019;21:085001.
10. Gevorgyan AH. Magnetically induced transparency in helically structured periodic crystals. Phys Rev E. 2022;105:014704.
11. Zhang X, Zou CL, Jiang L, Tang HX. Cavity magnomechanics. Sci Adv. 2016;2:e1501286.
12. Wang B, Liu ZX, Kong C, Xiong H, Wu Y. Magnon-induced transparency and amplification in pt-symmetric cavity-magnon system. Opt Express. 2018;26:20248–57.
13. Ockeloen-Korppi C, et al. Stabilized entanglement of massive mechanical oscillators. Nature. 2018;556:478–82.
14. Azimi Mousolou V, et al. Hierarchy of magnon mode entanglement in antiferromagnets. Phys Rev B. 2020;102:224418.
15. Yu M, Shen H, Li J. Magnetostrictively induced stationary entanglement between two microwave fields. Phys Rev Lett. 2020;124:213604.
16. Hu G, et al. Coherent steering of nonlinear chiral valley photons with a synthetic au–ws2 metasurface. Nat Photonics. 2019;12:467–72.
17. Zhong W, Zheng Q, Cheng G, Chen A. Nonreciprocal genuine steering of three macroscopic samples in a spinning microwave magnonical system. Appl Phys Lett. 2023;123:134003.
18. Guan SY, Wang HF, Yi XX. Cooperative-effect-induced one-way steering in open cavity magnonics. npj Quantum Inf. 2022;8:102.
19. Wang YP, et al. Bistability of cavity magnon polaritons. Phys Rev Lett. 2018;120:057202.
20. Wang F, Gou C, Xu J, Gong C. Hybrid magnon-atom entanglement and magnon blockade via quantum interference. Phys Rev A. 2022;106:013705.
21. Huang R, Miranowicz A, Liao JQ, Nori F, Jing H. Nonreciprocal photon blockade. Phys Rev Lett. 2018;121:153601.
22. Wang Y, Xiong W, Xu Z, Zhang GQ, You JQ. Dissipation-induced nonreciprocal magnon blockade in a magnon-based hybrid system. Sci China, Phys Mech Astron. 2022;65:260314.
23. Zhang X, et al. Magnon dark modes and gradient memory. Nat Commun. 2015;6:8914.
24. Bi M, Yan X, Xiao Y, Dai C. Magnon dark mode in a strong driving microwave cavity. J Appl Phys. 2019;126:173902.
25. Lu TX, Xiao X, Chen LS, Zhang Q, Jing H. Magnon-squeezing-enhanced slow light and second-order sideband in cavity magnomechanics. Phys Rev A. 2023;107:063714.
26. Li X, et al. Phase control of the transmission in cavity magnomechanical system with magnon driving. J Appl Phys. 2020;128:233101.
27. Leggett AJ. Macroscopic quantum systems and the quantum theory of measurement. Prog Theor Phys. 1980;69:80–100.
28. Degen CL, Reinhard F, Cappellaro P. Quantum sensing. Rev Mod Phys. 2017;89:035002.
29. Zhang H, et al. Breaking anti-pt symmetry by spinning a resonator. Nano Lett. 2020;20:7594–9.
30. Einstein A, Podolsky B, Rosen N. Can quantum-mechanical description of physical reality be considered complete. Phys Rev. 1935;47:777.
31. Shen RC, et al. Long-time memory and ternary logic gate using a multistable cavity magnonic system. Phys Rev Lett. 2021;127:183202.
32. Zhang G, Wang Y, You J. Theory of the magnon Kerr effect in cavity magnonics. Sci China, Phys Mech Astron. 2019;62:1–11.
33. Wollman EE, et al. Quantum squeezing of motion in a mechanical resonator. Science. 2015;349:952–5.
34. Lecocq F, Clark JB, Simmonds RW, Aumentado J, Teufel JD. Quantum nondemolition measurement of a nonclassical state of a massive object. Phys Rev X. 2015;5:041037.
35. Pirkkalainen JM, Damskägg E, Brandt M, Massel F, Sillanpää MA. Squeezing of quantum noise of motion in a micromechanical resonator. Phys Rev Lett. 2015;115:243601.
36. Pradana A, Chew LY. Entanglement of nitrogen-vacancy-center ensembles with initial squeezing. Phys Rev A. 2021;104:022435.
37. Qian H, Zuo X, Fan ZY, Cheng J, Li J. Strong squeezing of microwave output fields via reservoir-engineered cavity magnomechanics. Phys Rev A. 2024;109:013704.
38. Agarwal GS, Huang S. Strong mechanical squeezing and its detection. Phys Rev A. 2016;93:043844.
39. Jähne K, et al. Cavity-assisted squeezing of a mechanical oscillator. Phys Rev A. 2009;79:063819.
40. Kamra A, Belzig W, Brataas A. Magnon-squeezing as a niche of quantum magnonics. Appl Phys Lett. 2020;117:090501.
41. Li J, Zhu SY, Agarwal GS. Squeezed states of magnons and phonons in cavity magnomechanics. Phys Rev A. 2019;99:021801.
42. Zhang W, Wang T, Han X, Zhang S, Wang HF. Quantum entanglement and one-way steering in a cavity magnomechanical system via a squeezed vacuum field. Opt Express. 2022;30:10969–80.
43. Yurke B, et al. Observation of parametric amplification and deamplification in a Josephson parametric amplifier. Phys Rev A. 1989;39:2519.
44. Bai CH, Wang DY, Zhang S, Liu S, Wang HF. Engineering of strong mechanical squeezing via the joint effect between Duffing nonlinearity and parametric pump driving. Photon Res. 2019;7:1229–39.
45. Shen Z, et al. Experimental realization of optomechanically induced non-reciprocity. Nat Photonics. 2016;10:657–61.
46. Kronwald A, Marquardt F, Clerk AA. Arbitrarily large steady-state bosonic squeezing via dissipation. Phys Rev A. 2013;88:063883.
47. Huang S, Chen A. Mechanical squeezing in a dissipative optomechanical system with two driving tones. Phys Rev A. 2021;103:023501.
48. Sounas DL, Alù A. Non-reciprocal photonics based on time modulation. Nat Photonics. 2017;111:774–83.
49. Shen Y, et al. Single-photon diode by exploiting the photon polarization in a waveguide. Phys Rev Lett. 2011;107:173902.

50. Zhang S, et al. Thermal-motion-induced non-reciprocal quantum optical system. Nat Photonics. 2018;12:744–8.
51. Scheucher M, Hilico A, Will E, Volz J, Rauschenbeutel A. Quantum optical circulator controlled by a single chirally coupled atom. Science. 2016;354:1577–80.
52. Tang JS, et al. Nonreciprocal single-photon band structure. Phys Rev Lett. 2022;128:203602.
53. Christophe C, et al. Electromagnetic nonreciprocity. Phys Rev Appl. 2018;10:047001.
54. Zhao B, Zhou KX, Wei MR, Cao J, Guo Q. Nonreciprocal strong mechanical squeezing based on the Sagnac effect and two-tone driving. Opt Lett. 2024;49:486–9.
55. Guo Q, et al. Nonreciprocal mechanical squeezing in a spinning cavity optomechanical system via pump modulation. Phys Rev A. 2023;108:033515.
56. Chen J, Fan XG, Xiong W, Wang D, Ye L. Nonreciprocal entanglement in cavity-magnon optomechanics. Phys Rev B. 2023;108:024105.
57. Wang YP, et al. Magnon Kerr effect in a strongly coupled cavity-magnon system. Phys Rev B. 2016;22:224410.
58. Gardiner C, Zoller P. Quantum noise: a handbook of Markovian and non-Markovian quantum stochastic methods with applications to quantum optics. Berlin: Springer; 2004.
59. Vitali D, et al. Optomechanical entanglement between a movable mirror and a cavity field. Phys Rev Lett. 2007;98:030405.
60. Weedbrook C, et al. Gaussian quantum information. Rev Mod Phys. 2012;84:621.
61. DeJesus EX, Kaufman C. Routh-Hurwitz criterion in the examination of eigenvalues of a system of nonlinear ordinary differential equations. Phys Rev A. 1987;35:5288.
62. Potts CA, Varga E, Bittencourt VASV, Kusminskiy SV, Davis FP. Dynamical backaction magnomechanics. Phys Rev X. 2021;11:031053.
63. Tan HT, Li GX, Meystre P. Dissipation-driven two-mode mechanical squeezed states in optomechanical systems. Phys Rev A. 2013;3:033829.
64. Ullah M, Mikki S. Nonreciprocal microwave field transmission in a quantum magnomechanical system controlled by magnetostriction and Kerr nonlinearities. Phys Rev X. 2024;109:214303.

Publisher's Note